Secondary instability mode of a roll pattern and transition to spatiotemporal chaos in the Taylor-Dean system

Patrick Bot, Olivier Cadot, and Innocent Mutabazi
Laboratoire de Mécanique, Université du Havre, 25, Rue Philippe Lebon, Boîte Postale 540, F-76058 Le Havre Cedex, France
(Received 22 September 1997; revised manuscript received 26 May 1998)

The secondary instability mode and transition to a weak chaotic regime in a one-dimensional roll pattern have been investigated in the Taylor-Dean system. The spatiotemporal modulation of a roll pattern, called a *triplet* state in Phys. Rev. Lett. **64**, 1729 (1990), is quantitatively characterized using the demodulation technique by the Hilbert transform. A triplet pattern arises from the primary structure by a periodic modulation of the phase both in space and time. The amplitude of the modulation, chosen as an order parameter, has been measured, and it grows as a square root of the reduced control parameter. The correlation length and time of the triplet pattern are maximal near the threshold, and decrease to values comparable to the size and period of a triplet in the chaotic regime. In the chaotic regime, regular oscillations of triplets are observed with a finite frequency, suggesting a phase modulation of the triplet pattern itself. [S1063-651X(98)02209-0]

PACS number(s): 47.20.Lz, 47.27.Cn

I. INTRODUCTION

Pattern formation in nonlinear systems remains one of the challenging problems of contemporary physics [1,2]. Systems maintained far from thermodynamic equilibrium by external stresses show surprising organized structures, which may undergo successive transitions leading to chaos or weak turbulence. Each transition may be associated with a broken symmetry of the system [1,2]. The prototypes of such nonlinear systems are Rayleigh-Bénard convection and Taylor-Couette flow [3–6], which have been largely investigated by different experimental, numerical, and theoretical tools [1,2]. While transition scenarios to weak chaos in small size systems have been well defined [1], recent developments have been much concerned with spatially extended systems which exhibit spatiotemporal chaos that does not possess universal transition sequences. Depending on the control parameter and on the base state, an extended system can undergo a transition to either a stationary or an oscillatory pattern. Extended systems with a first instability giving an oscillatory pattern are of particular interest, since the transition to space-time chaos occurs not far from the onset of the primary bifurcation [1,2]. They are then more accessible to an easier modelization, which can allow a comparison between experimental and theoretical results. A transition to oscillatory pattern has been observed in Rayleigh-Bénard convection in fluids with small Prandtl numbers Pr [7], in convection with binary mixture fluids [8], in Taylor-Couette flow with counter-rotating cylinders [9], in a Taylor-Couette system with an axial flow [10], or in the Taylor-Dean system [11]. These observations in one-dimensional systems have been explained using the framework of the complex Ginzburg-Landau equation [12] and the Kuramoto-Sivashinsky equation [2]. Spatiotemporal patterns observed in different extended systems exhibit interesting features such as localized defects, isolated patches of traveling waves, holes [13], or solitons [14].

Recently, the Taylor-Dean system has been the subject of intense investigations because it exhibits a large variety of patterns [4,11,15,16]. The base flow may undergo a transition to either stationary Taylor-Couette and Dean modes or oscillatory modes of traveling rolls [17]. Under external forcing, it can exhibit a standing roll pattern [18]. In contrast with the Taylor-Couette system [5], the system does not have rotational symmetry around the cylinder axis. In fact, a partial filling of the gap produces two horizontal free surfaces that induce a pressure gradient along the azimuthal direction. Far from the cylinder ends, the base laminar flow is stationary and contains two flow parts: a recirculation zone near the free surfaces where the velocity field has two components, and a bulk flow in which the velocity field has only an azimuthal component [19].

Previous experimental studies of the Taylor-Dean system [11,15] mainly characterized the primary pattern of traveling inclined rolls; a qualitative description of the short wavelength modulation (called triplet) was given in Ref. [15]. In this paper, we give quantitative results about this transition, together with a qualitative description of higher instability modes. The secondary instability is confirmed to be a supercritical transition with an order parameter that has been measured. For higher values of the control parameter, the modulated pattern exhibits spatiotemporal defects and oscillations leading to a spatiotemporal chaos.

The paper is organized as follows: the experimental system with data acquisition and analysis tools is described in Sec. II. Section III addresses the description of results that are discussed in Sec. IV and Sec. V contains the conclusion.

II. EXPERIMENTAL SYSTEM

A. Description of the system and data acquisition

The considered Taylor-Dean system is similar to that used by Mutabazi *et al.* [15]. Briefly, it consists of two horizontal coaxial cylinders partially filled with water. The inner cylinder is made of black anodized aluminum (for a better visualization contrast) with a radius $a = 4.46$ cm. The outer cyl-

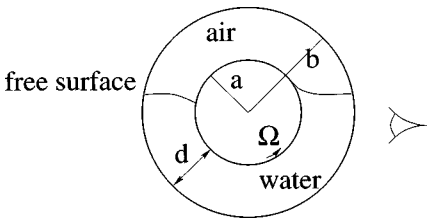

FIG. 1. Cross section of the partially filled cylindrical annulus in a horizontal position: $a=4.46$ cm, $b=5.08$ cm. The working length of the system $L=55$ cm.

inder is made of glass with a radius $b=5.08$ cm (Fig. 1). The gap between the cylinders is $d=b-a=0.62$ cm over a length $L=55$ cm. Hence the system has a radius ratio $\eta=a/b=0.878$, and an aspect ratio $\Gamma=L/d=90$. The filling level angle θ_f is chosen as $\theta_f/2\pi=0.7$.

The inner cylinder is rotated by a dc servomotor which is driven by a PC, while the outer cylinder remains fixed in the laboratory frame. Thus the only control parameter is the Reynolds number relative to the inner rotating cylinder defined as $\mathrm{Re}=\Omega ad/\nu$, where Ω is the cylinder angular frequency and ν the kinematic viscosity of the fluid.

The precision on the geometric dimensions and on the rotation frequency is better than 0.5%. Therefore, the main error on the control parameter Re comes from the viscosity fluctuations with temperature. During experiments, the temperature has been measured, and we estimated the uncertainty on the control parameter to be $\Delta\,\mathrm{Re}/\mathrm{Re}\sim 1\%$.

Teflon rings are attached at the ends of the inner surface of the fixed outer cylinder in order to reduce the effects of Ekman recirculation. The aspect ratio $\Gamma=90$ is large enough to consider the experimental system as an extended system [2]; actually more than 70 rolls are observed in the system. Moreover, the roll intensity vanishes slightly before the ends, suggesting that the roll pattern has soft boundaries.

For the experiments, we used distilled water with 1% Kalliroscope AQ1000 for the visualization. With a light from a fluorescent tube, the flow was visualized on the front side (Fig. 1). To obtain spatial information about the roll dynamics, a linear 1024-pixel charge coupled device (CCD) array records the reflected light intensity distribution $I(x)$ from a line along the axis of the cylinders, 1 cm below the free surface. The recorded length is 30 cm in the central part of the system corresponding to a spatial resolution of 34 pixels/cm. The intensity is sampled in 256 values, displayed in gray levels at regular time intervals along time axis to produce space-time diagrams $I(x,t)$ of the pattern. For a good resolution of frequency spectra, acquisitions of 8192 time steps of 0.2 s were used. Wave-number spectra have been averaged in time in order to improve their resolution. The data are processed on a UNIX workstation.

Times, lengths, and velocities are scaled, respectively, by the radial diffusion time $d^2/\nu\sim 40$ s, the gap size d, and the radial diffusion velocity $\nu/d\sim 0.016$ cm/s. All quantities used in this paper are dimensionless, unless stated differently. In experiments, in order to avoid spurious transient states, we waited 15 min between each variation of the control parameter from 260 up to 340 by a step $\Delta\,\mathrm{Re}=2$, while 30 min were required before each data acquisition.

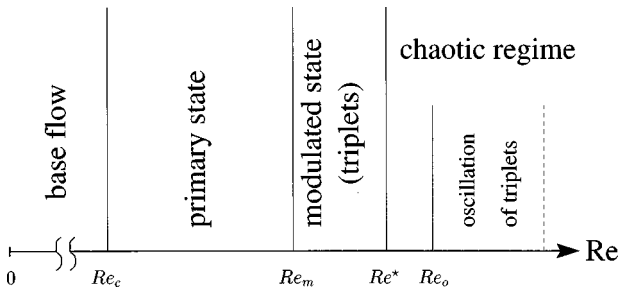

FIG. 2. Sequence of observed states ($\mathrm{Re}_c=260\pm 2$, $\mathrm{Re}_m=292\pm 2$, $\mathrm{Re}^*=307\pm 3$, $\mathrm{Re}_0=315\pm 3$).

B. Demodulation and statistical analysis

In order to quantify spatial and temporal variations of wave numbers and frequencies, we performed the demodulation technique by Hilbert transform [13] of the signal with respect to time. The real signal $I(x,t)$ is transformed in its complex equivalent expression as follows:

$$I(x,t)=\mathrm{Re}[\tilde{I}(x,t)], \tag{1}$$

where

$$\tilde{I}(x,t)=|A(x,t)|e^{i\phi(x,t)}.$$

In practice, the original signal $I(x,t)$ is first bandpass filtered in space with a relatively large band (elimination of large-scale lighting inhomogeneities and small-scale noise). Then a temporal fast Fourier transform is computed, and components of negative frequencies are set to zero with a smooth filter. The latter consists of a bandpass filter with a band carefully adapted to each pattern, centered on the roll frequency. Afterwards, the inverse Fourier transform of the truncated signal in the spectral space gives the amplitude $|A(x,t)|$ and the total phase $\phi(x,t)$. The wave numbers and frequencies are measured as the spatial and temporal phase gradients: $q(x,t)=\partial\phi/\partial x$ and $f(x,t)=(1/2\pi)(\partial\phi/\partial t)$.

Statistical analysis of the pattern signal has been performed for each value of Re: the probability density functions of local frequencies and wave numbers have been built over 4×10^5 values of phase gradients. Autocorrelation functions of the space-time signals have been calculated in order to obtain the correlation length and time of pattern.

III. RESULTS

A. Different states of the pattern

The sequence of states observed in this experiment is shown in Fig. 2. The space-time diagrams and corresponding frequency spectra of patterns observed are exhibited in Figs. 3–7 for different values of the control parameter from the primary state to chaotic regime. In addition to the roll frequency peaks, spectra contain the cylinder frequency f_i because a few Kalliroscope particles stick to the inner cylinder surface and periodically reflect the light to the CCD array.

The primary instability of the base flow occurs at $\mathrm{Re}_c=260\pm 2$, and gives rise to a pattern of traveling inclined rolls with a definite wave number $q_1=4.8\pm 0.1$ and frequency $f_1=18.90\pm 0.05$ corresponding to a drift velocity $v_d=24.7$ at the threshold. As reported in Ref. [11], the tran-

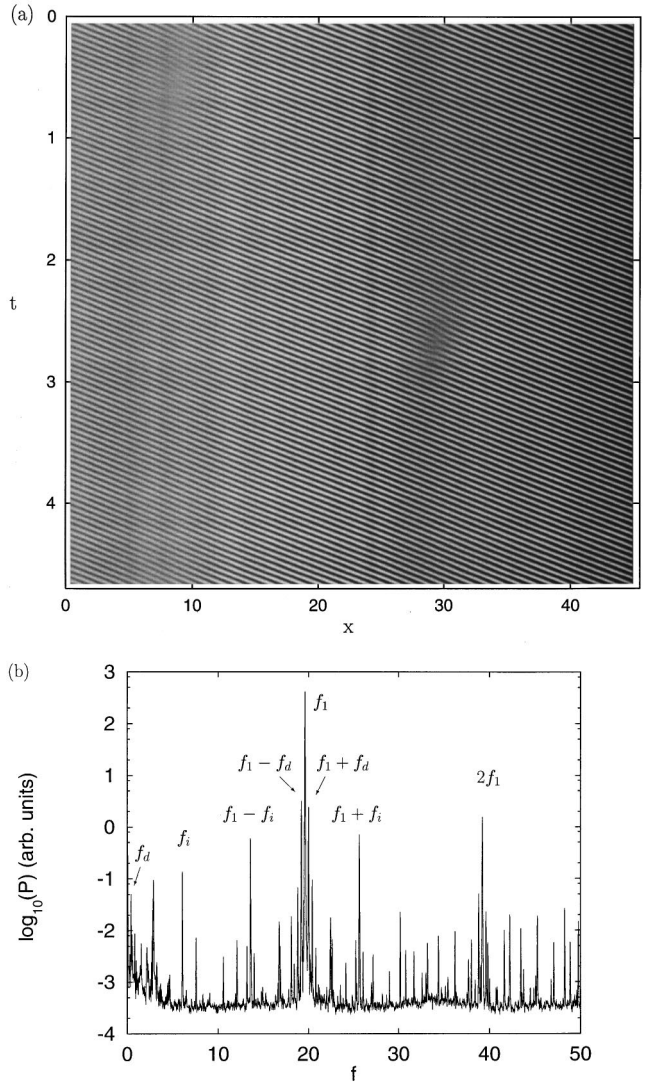

FIG. 3. (a) Space-time diagram of a primary roll pattern (Re $=272$). (b) Spatially averaged power spectral density (P): roll frequency $f_1=19.31$, f_i represents the inner cylinder rotation frequency, and the defect induced frequency $f_d=0.43$. The pattern contains two spatiotemporal defects at $x=8$, $t=0.5$ and $x=29$, $t=2.7$.

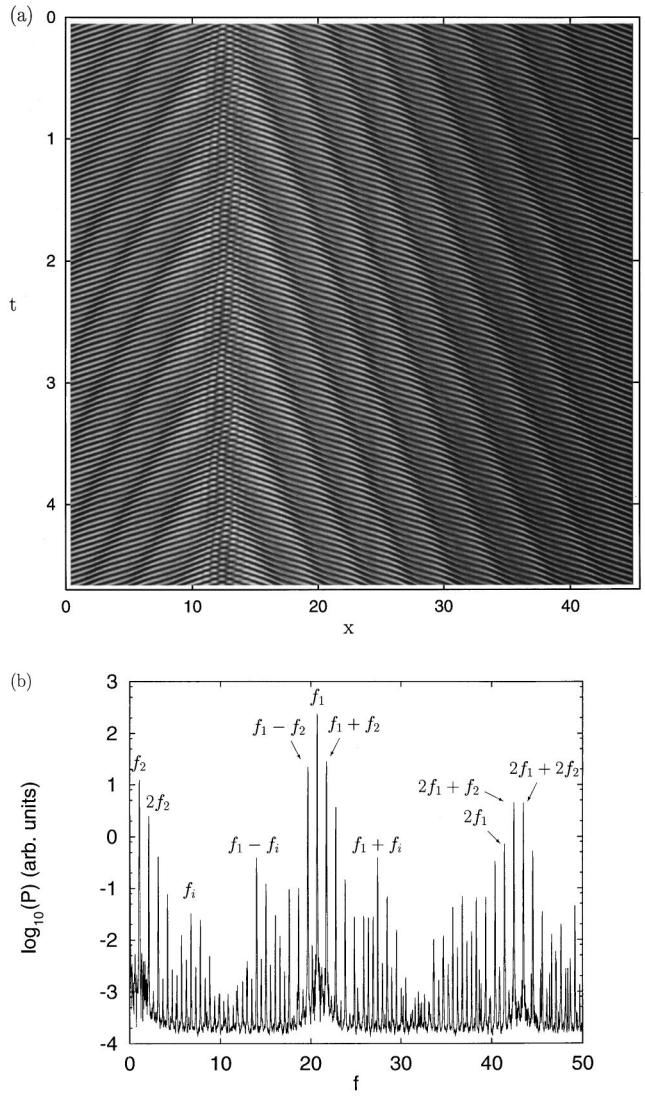

FIG. 4. (a) Space-time diagram of a modulated pattern (Re $=303$). (b) Spatially averaged power spectral density (P): modulation frequency $f_2=1.06$, and its coupling peaks with the roll frequency $f_1=20.72$.

sition is supercritical; no hysteresis in the threshold was found, within our experimental precision, when ramping up and down in the neighborhood of the onset. Localized spatiotemporal defects (mostly collisions between rolls) have been observed. A typical space-time diagram of the pattern in the primary state and corresponding frequency spectrum are shown in Figs. 3(a) and 3(b). As the system is extended, a source separating left and right traveling rolls may occur in the pattern just above the threshold of the primary instability. The appearance of sources and spatiotemporal defects and their density depend strongly on the ramping rate.

At $\mathrm{Re}_m=292\pm2$, the traveling roll pattern undergoes a secondary supercritical instability [15]. A spatiotemporal modulation occurs: the roll pattern becomes biperiodic in space and time [Figs. 4(a) and 4(b)]. In the space-time diagram, the wavelength modulation is characterized by oblique stripes due to periodic variation of the roll size. This modulation drifts with a velocity much smaller than that of individual rolls [Fig. 4(a)]. Visualizations of modulated pattern show that drift velocity and size of rolls change along the pattern. This modulation is characterized by a wave number $q_2=1.7\pm0.1$ and a frequency $f_2=1.10\pm0.05$ at threshold. Figure 4(b) shows peaks f_1 and f_2 and coupling peaks between f_1 and f_2. The ratio $q_1/q_2=2.8$ is close to 3, that is why the pattern was called *triplet* pattern previously [15]. For higher values of Re, the dynamics of the pattern is governed mainly by the triplets, which behave themselves as coherent objects.

For $\mathrm{Re}>\mathrm{Re}^*=307\pm3$ (Fig. 2), triplet patterns undergo long wavelength perturbations resulting in collisions between two triplets [Fig. 5(a)] similar to collisions between rolls. The frequency spectrum of the pattern with collision of triplets [Fig. 5(b)] contains more noise than the former spectrum of the periodic triplet regime [Fig. 4(b)]. For $\mathrm{Re}>\mathrm{Re}_o=315\pm3$, the spatiotemporal diagram contains domains of regular oscillations of the triplets separated by disordered domains (with defects and sources). Figure 6(a) shows one of such regular domains with a third definite frequency f_3 [Fig.

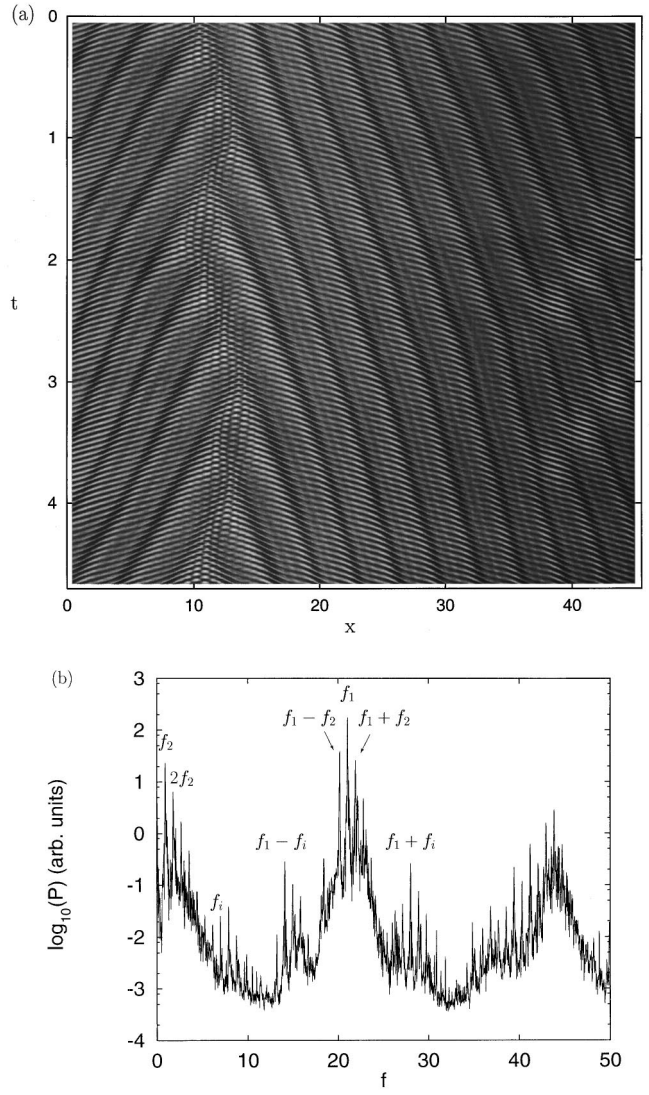

FIG. 5. (a) Space-time diagram of a modulated pattern with defects on triplets (Re=312). (b) Spatially averaged power spectral density (P) with background noise ($f_1=21.01$, $f_2=0.80$).

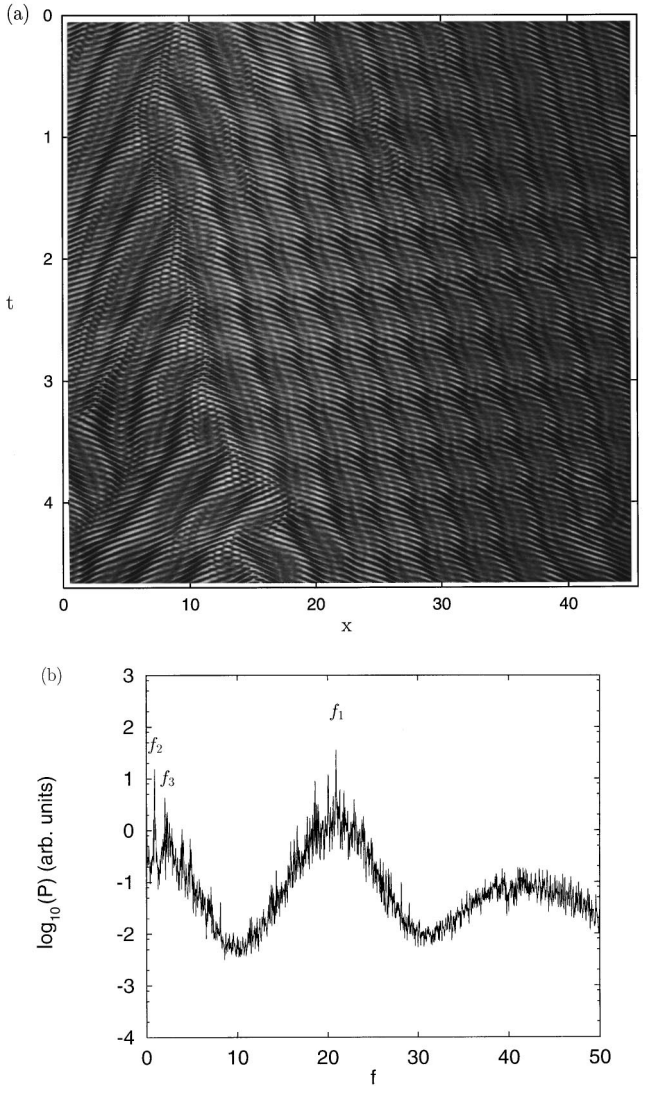

FIG. 6. (a) Space-time diagram of modulated pattern with oscillations on triplets (Re=326). (b) Power spectral density (P) with a background noise shows a peak $f_3=1.93$ of the triplet oscillations ($f_1=20.80$, $f_2=0.83$).

6(b)]. When Re increases, sources, sinks, triplets collision and creation events occur frequently in the pattern [Fig. 7(a)], and the measurement of f_3 becomes difficult as the pattern frequency spectrum contains a large background noise [Fig. 7(b)].

B. Description of the spatiotemporal modulated pattern

Figures 8(a) and 8(b) show the wave-number variations in space and in time, respectively. The wave number oscillates with a well defined wavelength $\Lambda=2\pi/q_2$ and period $T=1/f_2$. The amplitude of these oscillations is constant in time and almost constant in space. In the latter case, the fluctuations are due to weak long scale inhomogeneities of the pattern. We have analyzed the histograms of local wave numbers and frequencies, in order to measure the average amplitude of the wave-number oscillations in the whole modulated pattern. This has been determined by the difference Δq separating the two peaks: $\Delta q=q_{\max}-q_{\min}$ (Fig. 9). The peaks around $q_{\min}$ and $q_{\max}$ correspond, respectively, to small and large rolls in the pattern. Similarly, the histograms of frequencies exhibit two peaks at frequencies $f_{\min}$ and $f_{\max}$ and yield the amplitude of the frequency variation $\Delta f=f_{\max}-f_{\min}$. The peaks' disymmetry is related to higher harmonics of the wave-number oscillations, and their width to previously mentioned inhomogeneities [Fig. 8(a)].

The spatial or temporal variation of frequency and wave number indicates that the triplet pattern may be considered as a wave envelope with a group velocity v_g defined as

$$v_g=2\pi\frac{df}{dq}=2\pi\frac{df}{dx}\Big/\frac{dq}{dx}.$$

From the data for the wave number $q(x)$ and the frequency $f(x)$ just above the onset of the phase modulation, we have obtained the group velocity $v_g=4.2\pm0.4$. This value is the same as that measured directly from the space-time diagram of triplets [Fig. 4(a)].

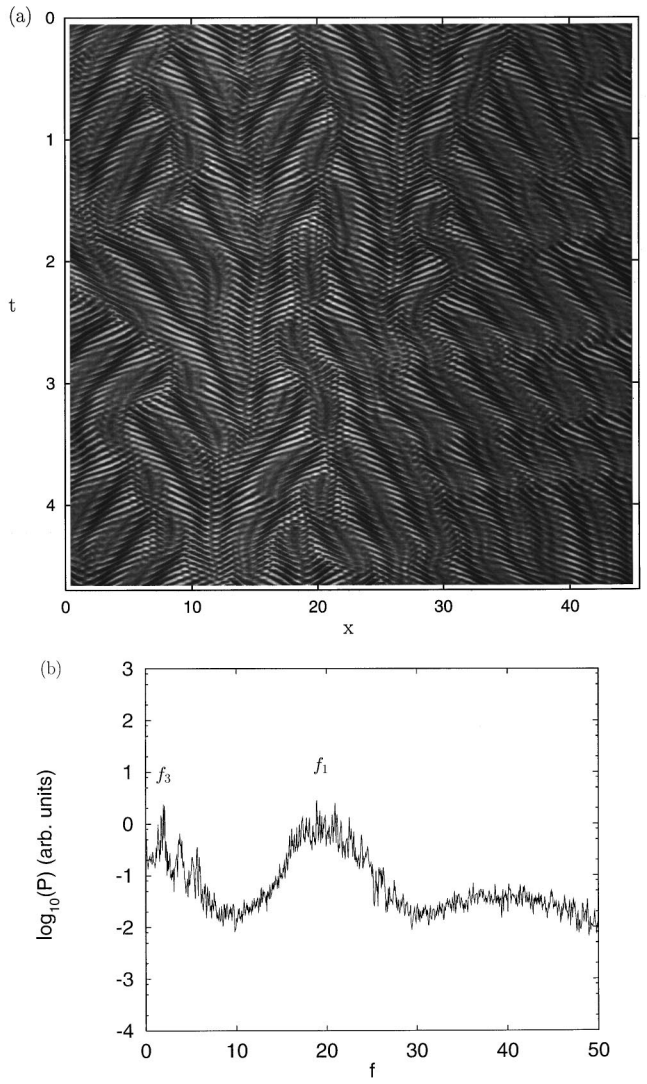

FIG. 7. (a) Space-time diagram of triplet pattern with defects and oscillations (Re=343). (b) Power spectral density (P) shows a large background noise, in which are immersed peaks of frequencies f_1, f_2, and f_3.

C. Variation of frequency and wave number with Re

Figure 10 shows all the measured frequencies (a) and wave numbers (b) for Re$\in$[260,340]. The frequency f_1 increases monotonously with Re [Fig. 10(a)], while the wave number q_1 is constant within long wavelength perturbations [Fig. 10(b)]. Above the onset of modulation (Re>Re$_m$), the modulation frequency f_2 and wave number q_2 vary weakly with the control parameter.

For Re>Re$_m$, we have plotted on the same diagrams extremal values of frequency and wave number of the modulated pattern. The mean roll frequency is $f_1 \approx (f_{\max} + f_{\min})/2$, and f_2 is the modulation frequency that remains almost constant, while $\Delta f = f_{\max} - f_{\min}$ is the amplitude of frequency modulation and increases with the control parameter [Fig. 10(a)]. The same observation holds for the wave numbers.

The oscillations of the triplets have a frequency f_3, which appears to be almost constant with respect to Re in the range [315,340]. The frequency f_3 is not a harmonic of f_2. The

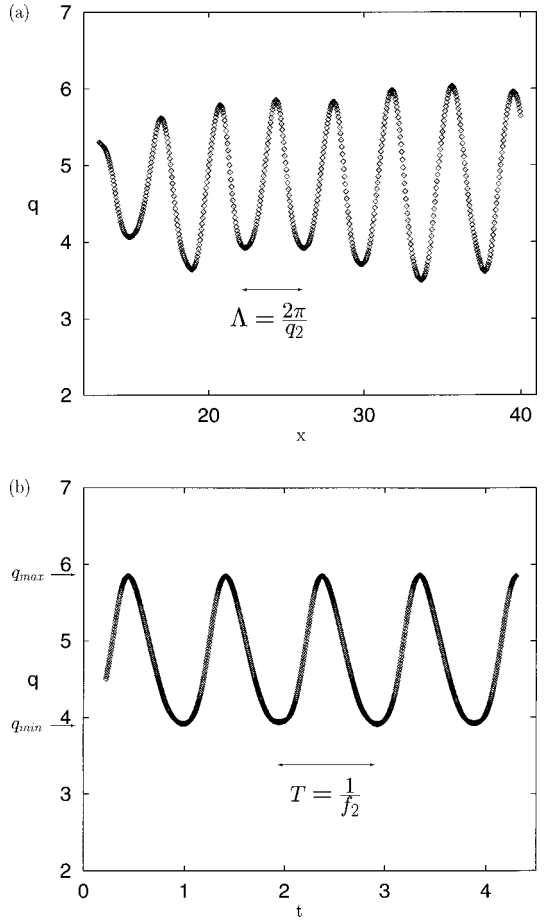

FIG. 8. Periodic variation of the roll wave number of the modulated pattern at Re=303: (a) in space with a wavelength $\Lambda = 2\pi/q_2$, and (b) in time with a period $T = 1/f_2$. The spatial profile of the wave number has large-scale inhomogeneities.

wave number associated with these oscillations is not accessible from the spectra; it has been estimated from the space-time diagram. We have found that $q_3 \approx 0.18$ corresponding to a spatial period of 35 that is close to the visualization length.

D. Pattern correlation length and time

We have measured the correlation length ξ and time τ from the autocorrelation function of the pattern signal. For

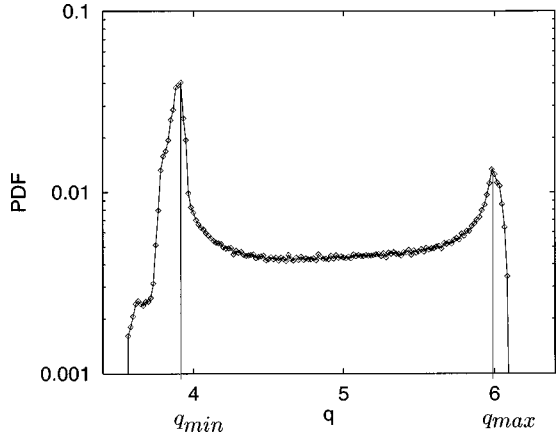

FIG. 9. Probability density functions (PDF) of the local wave number in a modulated pattern at Re=303.

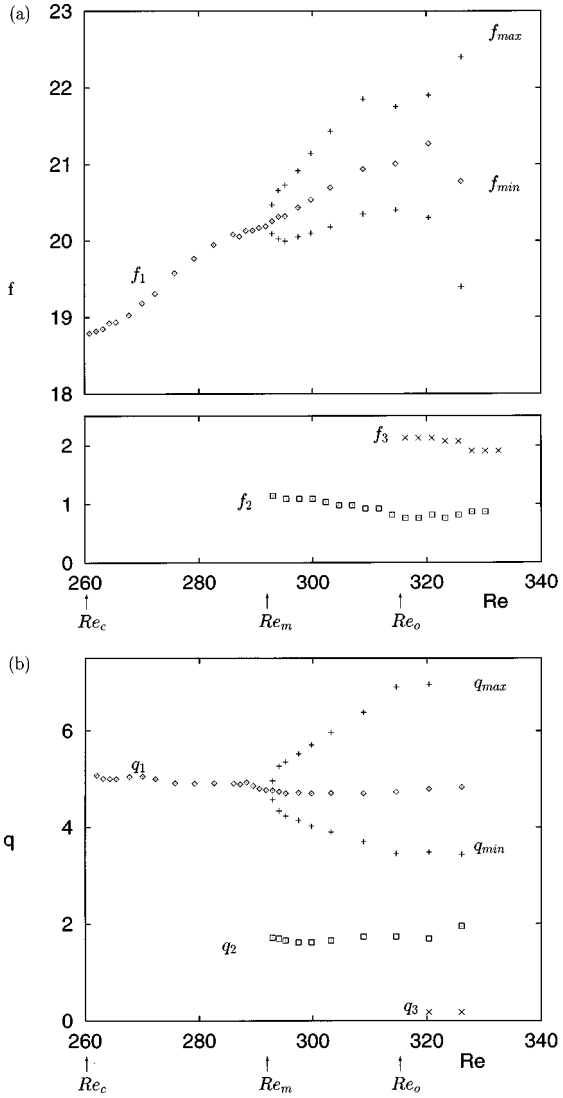

FIG. 10. Variation with the control parameter Re of (a) the frequency and (b) the wave number.

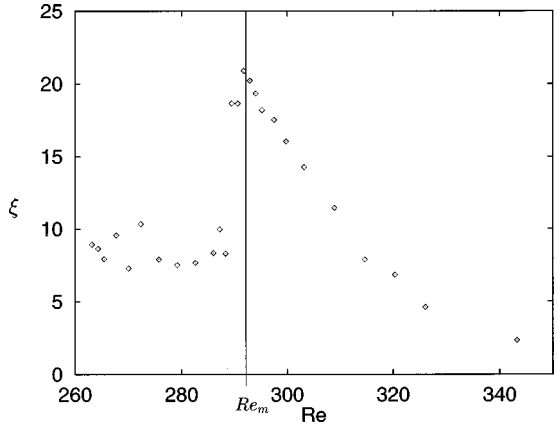

FIG. 11. Correlation length, as a function of Re: the onset of the spatiotemporal modulation is characterized by a sharp increase of the correlation length of the pattern.

Re$<$Re$_m$ the correlation corresponds to rolls, while for Re $>$Re$_m$ it is associated with the triplets. In the primary state, the correlation length $\xi \approx 8$ (six rolls), these data (Fig. 11) are scattered because of spatiotemporal defects and source in the pattern [15]. Just before the spatiotemporal modulation sets in, the pattern has no more defect and its correlation length increases up to $\xi = 19$ (15 rolls). The correlation length and time reach maximal values near the threshold of the modulation. Just above the onset of the spatiotemporal modulation (Re$>$Re$_m$), the correlation length covers five triplet wavelengths. Before and above the pattern modulation, the correlation length remains lower than the total size of the pattern because of the presence of a source and long-scale inhomogeneities. Actually, the size of the pattern on the right side of the source is about 20 triplet wavelengths. The correlation time near Re$=$Re$_m$ is about 13 triplet periods. Away from the onset, the correlation length and time of the triplet pattern decrease to values comparable with the size or the period of a triplet.

IV. DISCUSSION

A. Primary state pattern

The first instability gives rise to traveling inclined rolls, showing the parity breaking of the roll pattern. The drift velocity of rolls increases almost linearly with the control parameter. Both facts suggest that this first transition can be interpreted as a drift instability due to a coupling of the fundamental mode with its harmonics [20,21]. Similar mechanisms of parity breaking have been observed in the Taylor-Dean system with a rotating outer cylinder [22], and in other experimental systems such as printer instability [23].

The frequency of the roll pattern is constant along the system axis, while the wave number fluctuates around $q_1 = 4.8$ because of pattern inhomogeneities that induce spatiotemporal defects [Fig. 3(a)]. In fact, the wave number varies along the system axis within $\delta q = 0.25$, corresponding to long scale perturbations of length $L_r = 2\pi/\delta q = 25$, which is comparable with the size of the subsystem of right traveling rolls. In the spectrum of Fig. 3(b), we can see a low frequency f_d, and related satellite peaks around f_1. These peaks are due to the presence of defects in the pattern. This is a typical characteristic of a Benjamin-Feir instability [1]. The presence of spatiotemporal defects in the primary pattern is responsible for the strong fluctuations of the correlation length and time. No defect has been observed when approaching the modulation threshold, the pattern becomes phase stable relative to long-scale perturbations [24,25].

B. Phase modulation

Within our experimental precision, the transition to spatiotemporal modulation is supercritical; no significant hysteresis was found ramping up and down around Re$=$Re$_m$, in agreement with previous study [15]. We have quantitatively confirmed the supercritical nature of the secondary transition. In fact, since this modulation affects the phase of the pattern, we have chosen the amplitude of wave-number modulation $\Delta q = q_{\max} - q_{\min}$ as the order parameter for the transition. It measures the wave-number spreading, and therefore the phase perturbation strength to the primary pat-

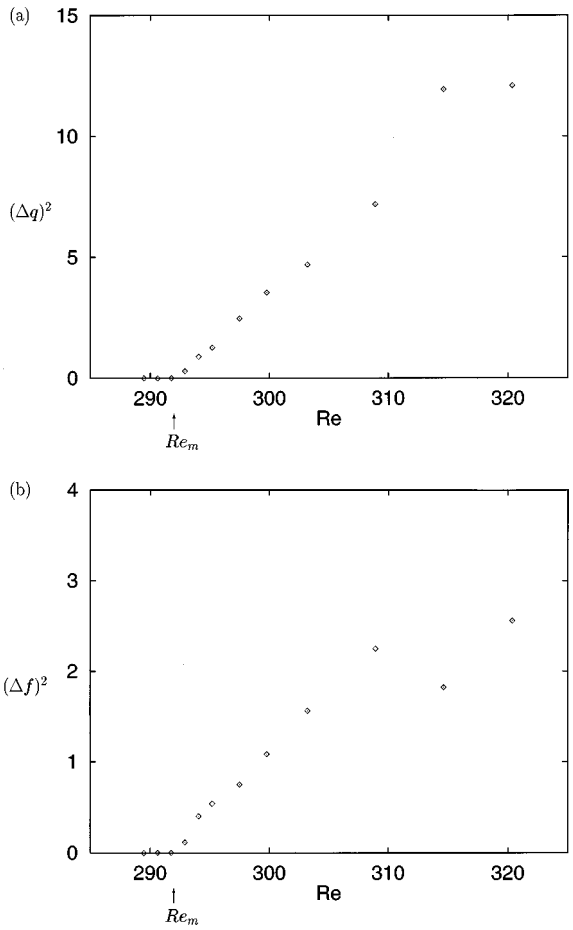

FIG. 12. Variation with the control parameter Re of the modulation amplitude (order parameter): (a) wave number, (b) frequency.

tern. For small values of the reduced control parameter $\varepsilon = (\mathrm{Re} - \mathrm{Re}_m)/\mathrm{Re}_m$, the dependence of Δq with ε was fitted by a power law [Fig. 12(a)]:

$$\Delta q = 2.4 q_1 \varepsilon^{0.50 \pm 0.02}.$$

Similarly, the amplitude of the frequency modulation $\Delta f = f_{\max} - f_{\min}$ has a power law behavior [Fig. 12(b)]:

$$\Delta f = 0.3 f_{1m} \varepsilon^{0.50 \pm 0.15},$$

where f_{1m} is the roll frequency measured at the modulation threshold.

As the modulation sets in, the size and the drift velocity of individual rolls change periodically in space and time with a finite wave number q_2 and a finite frequency f_2. The fact that q_2 and f_2 do not vary significantly with the control parameter Re is a signature that they are inherent to a secondary instability mode of the pattern. A similar behavior was observed by Flesselles, Croquette, and Jucquois [13] in a study of the transition to chaos in a chain of nonlinear coupled oscillators.

Close to the onset Re_m, the total phase of the periodic modulated pattern in space and time, traveling to the right, can be described by the following expression

$$\Phi(x,t) = \omega_1 t - q_1 x + \varphi(x,t), \tag{2}$$

where

$$\varphi(x,t) = \alpha \cos(\omega_2 t - q_2 x),$$

where $\omega_j = 2\pi f_j$ $(j = 1,2)$ is the angular frequency. This function represents a sinusoidal modulated phase in time and space. The particular case $\alpha = 0$ represents the primary state. Therefore, α is related to the order parameter Δq or Δf as follows: $\alpha = \Delta q / 2 q_2 = \Delta f / 2 f_2$. Spatiotemporal plots of the phase from expression (2) with experimental values ω_1, q_1, ω_2, and q_2 reproduce patterns very similar to those observed in experiment [Figs. 13(a) and 13(b)]. The higher harmonics observed in the phase modulation are not taken into account in relation (2).

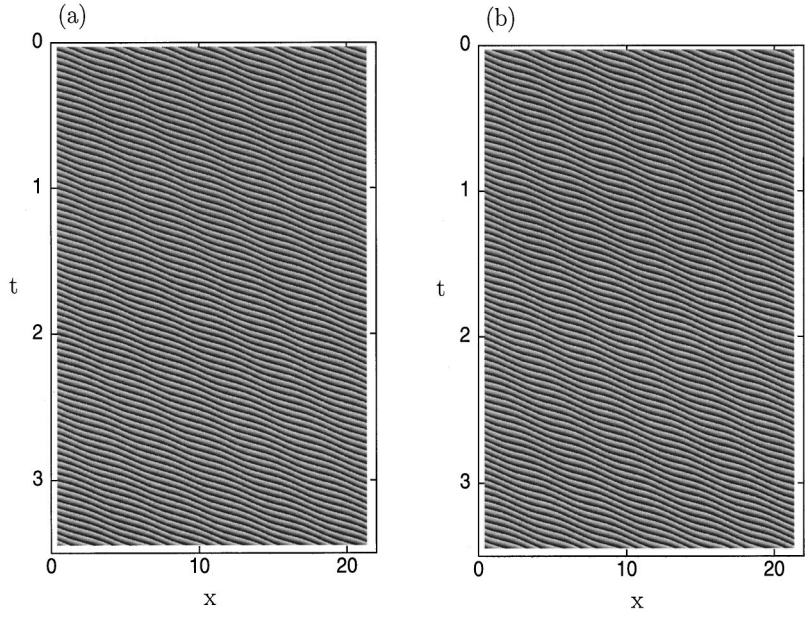

FIG. 13. Space-time diagram of a pattern phase: (a) experimental pattern at Re=303; (b) pattern given by function (2), for $\alpha = 0.8$.

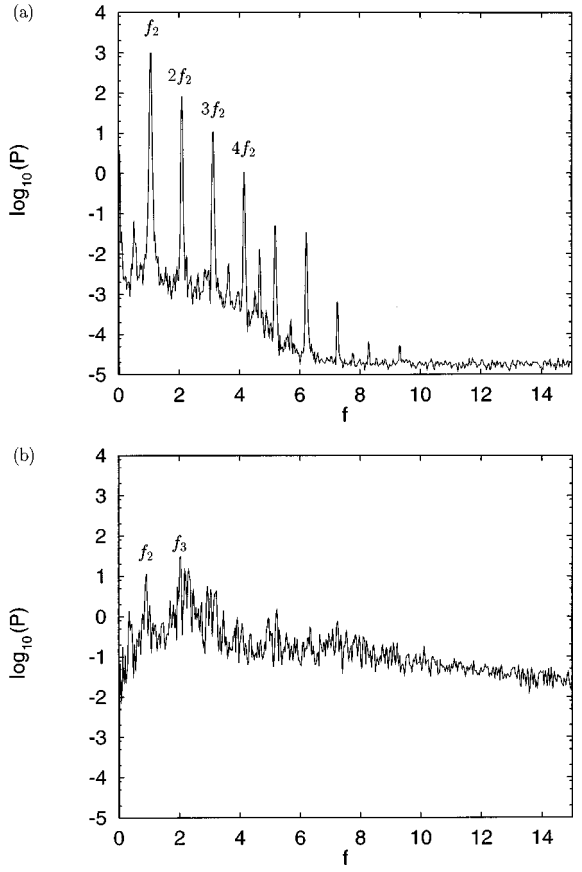

FIG. 14. Power spectral density (P) of the phase gradient signal $q(t)$: (a) in the regular triplet state at Re=303; (b) in the chaotic regime at Re=326.

C. Chaotic regime

As the control parameter is increased away from Re_m, the triplet pattern becomes unstable to long wavelength perturbations that lead to spatiotemporal defects on triplets. We have observed that triplet patterns are very sensitive to perturbations from the system boundaries.

The oscillations of triplets may be interpreted as a phase modulation of the triplet pattern. Figure 6(a) shows that the oscillations travel to the left when the triplets drift to the right. Naively, the phase of the pattern could be represented as follows:

$$\varphi(x,t)=\alpha\ \cos[\omega_2 t-q_2 x+\beta\ \cos(\omega_3 t+q_3 x)], \qquad (3)$$

where β is an amplitude of the triplet oscillation. Although the amplitude β grows with the control parameter, we have not obtained satisfactory measurements of this growth because the oscillations are observed inside a chaotic regime.

The chaotic pattern is characterized by small values of the correlation length and time [1] compared to those of the whole system, and by a high level of the background noise in the spectra (Figs. 5–7). Figures 3–7 show qualitative changes from discrete to continuous spectra. In order to quantify this spectra evolution with the control parameter, we define a measure of noise. Since relevant information is contained in the phase, we quantify the noise from the spectra of phase gradient signal [such as Figs. 14(a) and 14(b)] as follows:

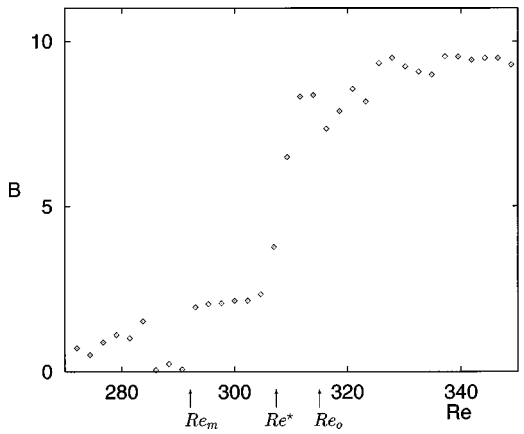

FIG. 15. Variation of the background noise with the control parameter: the value Re* separates domains of low and large phase noises.

$$B=\int_0^{f_N}\log_{10}\left\{\frac{S(f)}{S_0(f)}\right\}df,$$

where f_N is the Nyquist frequency, $S(f)$ is the power spectral density of the phase gradient signal $q(t)$, and $S_0(f)$ is that of the signal with the lowest noise (in our case at Re =288). The background noise B shows qualitative changes of the pattern dynamics (Fig. 15): it increases with the control parameter (except in the region where there are no defects). In particular, it grows drastically near Re=Re* because of the occurrence of defects on triplets. The value Re* ($\sim$307) corresponds to the transition to a continuous spectrum, characteristic of a chaotic regime.

The thresholds of successive transitions are close to the threshold Re_c of the primary instability; this is a typical property of patterns in extended systems [1,2]. In fact, the spatiotemporal chaotic regime occurs near $\mu=(\mathrm{Re}-\mathrm{Re}_c)/\mathrm{Re}_c=0.2$. A further investigation of the chaotic regime by different tools is underway, especially in the neighborhood of the triplets defects.

V. CONCLUSION

A transition scenario to spatiotemporal chaos in the Taylor-Dean system with a fixed outer cylinder has been investigated. The secondary instability of traveling inclined rolls gives rise to a triplet pattern with finite wave number and frequency that vary weakly with the control parameter. This supercritical transition is a spatiotemporal modulation with an order parameter chosen as the amplitude of the wave number or frequency variation. In modulated patterns, triplets are the appropriate basic structures; they undergo instabilities similar to those of rolls. Spatiotemporal defects and domains of regular oscillations of triplets have been observed in the chaotic regime. The correlation length and time of the pattern become smaller than those of a single triplet. The variation of the phase noise with the control parameter indicates qualitative changes of the pattern, and allows one to determine approximately the onset of the spatiotemporal

chaos in the system. For higher values of the control parameter, the triplet pattern exhibits a large number of defects, the dynamics of which necessitates a detailed investigation. Our study leaves open the question of the origin of the spatiotemporal modulation in the Taylor-Dean system. It calls for a theoretical analysis in the phase dynamics framework. Moreover, the recirculation zone of the base flow may play some role in the selection of the wave number q_2.

ACKNOWLEDGMENTS

The authors would like to thank Jean-Marc Flesselles and Arnaud Chiffaudel for interesting discussions on some aspects of results presented here. This work was supported by a grant from the Direction des Recherches et Etudes Techniques (DRET). One of us (P.B.) acknowledges the support from the MENESR.

[1] P. Manneville, *Structures Dissipatives, Chaos et Turbulence* (Aléa, Saclay, 1991). The English version was published under the title *Dissipative Structures and Weak Turbulence* (Academic, New York, 1990).
[2] M. Cross and P. C. Hohenberg, Rev. Mod. Phys. **65**, 851 (1993).
[3] S. Chandrasekhar, *Hydrodynamic and Hydromagnetic Stability* (Clarendon, Oxford, 1961).
[4] P. G. Drazin and W. H. Reid, *Hydrodynamic Stability* (Cambridge University Press, Cambridge, 1981).
[5] P. Chossat and G. Iooss, *The Couette-Taylor Problem* (Springer-Verlag, New York, 1994).
[6] E. L. Koschmieder, *Bénard Cells and Taylor Vortices* (Cambridge University Press, Cambridge, 1992).
[7] V. Croquette, Contemp. Phys. **30**, 113 (1989).
[8] P. Kolodner, D. Bensimon, and C. M. Surko, Phys. Rev. Lett. **60**, 1723 (1988).
[9] C. D. Andereck, S. S. Liu, and H. L. Swinney, J. Fluid Mech. **164**, 155 (1986).
[10] P. Büchel, M. Lücke, and D. Roth, Phys. Rev. E **53**, 4764 (1997). See also A. Tzameret and V. Steinberg, *ibid.* **49**, 4077 (1994) or K. L. Babcock, G. Ahlers, and D. S. Cannell, *ibid.* **50**, 3670 (1994).
[11] I. Mutabazi, J. J. Hegseth, C. D. Andereck, and J. E. Wesfreid, Phys. Rev. A **38**, 4752 (1988).
[12] H. R. Brand, P. S. Lombdahl, and A. C. Newell, Physica D **23**, 345 (1986). See also T. Passot and A. C. Newell, *ibid.* **74**, 301 (1994).
[13] J. M. Flesselles (private communication). See also J. M. Flesselles, V. Croquette, and S. Jucquois, Phys. Rev. Lett. **72**, 2871 (1994); J. Lega, B. Janiaud, S. Jucquois, and V. Croquette, Phys. Rev. A **45**, 103 (1992).
[14] O. Thual and S. Fauve, J. Phys. (France) **49**, 1829 (1988).
[15] I. Mutabazi, J. J. Hegseth, C. D. Andereck, and J. E. Wesfreid, Phys. Rev. Lett. **64**, 1729 (1990).
[16] I. Mutabazi, C. Normand, H. Peerhossaini, and J. E. Wesfreid, Phys. Rev. A **39**, 763 (1989). See also F. Chen and M. H. Chang, J. Fluid Mech. **243**, 443 (1992).
[17] P. Laure and I. Mutabazi, Phys. Fluids **6**, 3630 (1994).
[18] S. G. T. Tennakoon, C. D. Andereck, J. J. Hegseth, and H. Riecke, Phys. Rev. E **54**, 5053 (1996).
[19] C. Normand, I. Mutabazi, and J. E. Wesfreid, Eur. J. Mech. B/Fluids **10**, 335 (1991). See also K. S. Chen, A. C. Ku, T. M. Chan, and S. Z. Yang, J. Fluid Mech. **213**, 149 (1990). Very recently, the same problem was analyzed from a mathematical point of view by P. H. Gaskell, M. D. Savage, and M. Wilson, *ibid.* **337**, 263 (1997).
[20] S. Fauve, S. Douady, and O. Thual, J. Phys. II **1**, 311 (1991).
[21] M. R. Proctor and C. A. Jones, J. Fluid Mech. **188**, 301 (1988).
[22] I. Mutabazi and C. D. Andereck, Phys. Rev. Lett. **70**, 1429 (1993); Phys. Rev. E **51**, 4380 (1995).
[23] M. Rabaud, S. Michalland, and Y. Couder, Phys. Rev. Lett. **64**, 184 (1990).
[24] D. Walgraef, *Spatio-Temporal Pattern Formation* (Springer, New York, 1996).
[25] B. I. Shraiman, Phys. Rev. Lett. **57**, 325 (1986). See also H. Chaté and P. Manneville, *ibid.* **58**, 112 (1987).